Anisotropic homogeneous linewidth of the heavy-hole exciton in (110)-oriented GaAs quantum wells

Rohan Singh, Travis M. Autry, Gaël Nardin, Galan Moody, Hebin Li, Klaus Pierz, Mark Bieler, and Steven T. Cundiff

Phys. Rev. B **88**, 045304 — Published 8 July 2013

DOI: 10.1103/PhysRevB.88.045304

Anisotropic Homogeneous Linewidth of the Heavy Hole Exciton in (110)-Oriented GaAs Quantum Wells

Rohan Singh,[1,2] Travis M. Autry,[1,2] Gaël Nardin,[1] Galan Moody,[1,2]
Hebin Li,[1] Klaus Pierz,[3] Mark Bieler,[3] and Steven T. Cundiff[1,2,*]

[1] *JILA, University of Colorado & National Institute of Standards and Technology, Boulder CO 80309-0440*
[2] *Department of Physics, University of Colorado, Boulder CO 80309-0390*
[3] *Physikalisch-Technische Bundesanstalt, Bundesallee 100, D-38116 Braunschweig, Germany*

(Dated: June 27, 2013)

The homogeneous and inhomogeneous linewidths of the heavy hole exciton resonance in a (110)-oriented GaAs multiple quantum well sample have been measured using optical two-dimensional Fourier transform spectroscopy. By probing the optical nonlinear-response for polarization along the in-plane crystal axes [1$\bar{1}$0] and [001], we measure different homogeneous linewidths for the two orthogonal directions. This difference is found to be due to anisotropic excitation-induced dephasing, caused by a crystal-axis dependent absorption coefficient. The extrapolated zero-excitation density homogeneous linewidth exhibits an activation-like temperature dependence. We find that the homogeneous linewidth extrapolated to zero excitation density and temperature is ~ 34 μeV while the inhomogeneous linewidth is ~ 1.9 meV for both polarizations.

PACS numbers: 71.35.-y, 78.67.De, 78.47.jh

GaAs quantum wells (QWs), especially (001)-oriented QWs, have been studied extensively using ultrafast spectroscopy techniques.[1,2] For example, the dephasing time of the heavy hole (HH) exciton resonance was measured from transient four-wave mixing (FWM) experiments.[3] Improved growth techniques have led to a reduction in the inhomogeneous linewidth from a few[4] to less than an meV.[5]

More recently, there has been significant interest in (110)-oriented GaAs QWs. Very long spin relaxation times[6,7] and generation of spin currents by optical excitation[8] in these nanostructures find applications in THz generation[9] and spintronics. In coherent control experiments, carrier dephasing rates influence the optically generated currents in bulk GaAs[10] and (001)-oriented QWs.[11] A recent coherent control study on (110)-oriented GaAs QWs revealed novel photocurrents that directly depend on exciton polarization dephasing.[12] The contribution of excitons to spin currents[13] and the electron spin relaxation time[14] were also inferred. However, a clear understanding of excitonic effects in these QWs is lacking. While it is known that (110)-orientation has a profound influence on spin scattering rates in GaAs QWs,[6] it is not known if exciton scattering is also affected. Hence knowledge of dephasing time of excitons is critical to understanding excitonic effects in (110)-oriented QWs. To the best of our knowledge, the exciton dephasing times have not previously been reported for (110)-oriented GaAs QWs.

Optical fields are used to drive inter-band electronic transitions from the HH or light hole (LH) valence bands to the conduction band in QWs. The optical properties of semiconductor QWs are affected significantly by the symmetry of the heterostructure. For a (110)-oriented GaAs QW, where the QW itself is symmetric, the in-plane symmetry is reduced to C_{2v} point group compared to T_d for bulk GaAs and D_{2d} for an undoped (001)-oriented GaAs QW. The reduced symmetry results in the different spin (angular momentum) states of the conduction (valence) bands being split in k-space along the [1$\bar{1}$0] crystal axis while no splitting exists along the [001] crystal axis,[15,16] and, along with the k-linear terms of the transition dipole moment, contributes to the generation of spin currents.

The schematic band structures for the first conduction ($s_z = \pm 1/2$) and HH valence ($j_z = \pm 3/2$) bands along the X and Y directions are shown in Figs. 1(a) and 1(b), respectively. s_z and j_z are the projections, on the Z-axis, of the spin of an electron and the total angular momentum of a HH, respectively. We use a co-ordinate system with the X, Y and Z axes aligned along the [001], [1$\bar{1}$0] and [110] crystal axes, respectively, of the sample.

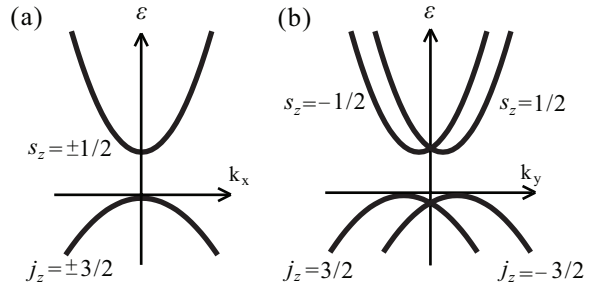

FIG. 1. An illustration of the energy levels for the conduction and HH valence bands in (110)-oriented GaAs QWs, as a function of wave vector along [001] (k_x) and [1$\bar{1}$0] (k_y) directions are shown in (a) and (b), respectively. The energy ε is shown for the conduction (HH valence) bands with spin (angular momentum) states $s_z = \pm 1/2$ ($j_z = \pm 3/2$).

Another consequence of the reduced symmetry is unequal transition dipole moments, and thus unequal absorption coefficients, for the exciton states polarized along the X and Y axes in the QW plane due to mixing of the HH and LH valence bands.[17,18] This anisotropy af-

fects the homogeneous linewidth, which is inversely proportional to the dephasing time, of the HH exciton transition.

In this paper, we report measurements of the homogeneous and inhomogeneous linewidths of the HH exciton state, using optical two-dimensional Fourier transform (2DFT) spectroscopy, in a (110)-oriented GaAs QW sample for excitation polarized along X and Y directions in the plane of the QW. The sample comprises 10 periods of 8 nm wide QWs separated by 8 nm wide $Al_{0.3}Ga_{0.7}As$ barriers, which has a lattice constant almost equal to that of GaAs.[19] The well-matched lattice constants result in small strain build-up in the grown heterostructure. It was mounted on a sapphire disk and the substrate was removed by selective etching for experiments in a transmission geometry. We find that while unequal absorption coefficients give rise to anisotropic excitation-induced dephasing (EID) effects, and thus different homogeneous linewidths for excitons excited along the two polarization directions, the extrapolated zero-excitation density homogeneous linewidth is the same for excitations along both directions. A study of the temperature dependence of the homogeneous linewidth reveals an activation-like behavior of thermal broadening. We also compare the results we obtain with those reported for (001)-oriented GaAs QWs to contrast the exciton dephasing mechanisms in QWs grown along the two growth directions.

Optical 2DFT spectroscopy is an extension of the three pulse transient FWM technique.[20] The extensions are sub-wavelength phase stabilization of the excitation pulses as a time delay is scanned and measurement of the signal field rather than the intensity. The phase stabilization enables us to unwrap the signal into two spectral dimensions by performing a numerical Fourier transform along the scanned time delay. An advantage of 2DFT spectroscopy is that we can simultaneously extract the homogeneous and inhomogeneous linewidths from a single spectrum. It is also possible to obtain the real part of the complex signal, which gives us insight into the contributions to the signal arising from many-body interactions.

The experimental details along with the set-up have been discussed elsewhere;[21] we present a brief description of the set-up here. The sample is kept in a cold finger continuous flow helium cryostat. As shown in Fig. 2(a), three excitation pulses A, B and C are incident on the sample with wave vectors $\mathbf{k}_A$, $\mathbf{k}_B$ and $\mathbf{k}_C$, respectively. The signal is emitted in the phase matched direction $\mathbf{k}_S = -\mathbf{k}_A + \mathbf{k}_B + \mathbf{k}_C$, which ensures that pulse A acts as a conjugate pulse. The signal is interfered with a reference pulse in a spectrometer and detected via spectral interferometry by a charge-coupled device camera with a spectral resolution of 17 μeV. The excitation pulses have a Gaussian intensity profile, and are focused on the sample with a spot $\sim$ 50 μm in diameter. The pulses are $\sim$ 120 fs long and are obtained from a 76 MHz repetition rate mode-locked Ti:sapphire laser. All the excitation beams are set to have, on an average, equal photon density per pulse, and, for the results presented here, the same linear polarization (X or Y). The polarization of the signal is also analyzed to be the same as that of the excitation pulses. We will refer to the polarization of all the excitation pulses and the signal as the polarization scheme. For example, polarization scheme X would mean that all the excitation pulses and the signal are polarized along the X axis. Figure 2(b) shows the sequence in which the excitation pulses are incident on the sample. Pulse A is incident on the sample first followed by pulses B and C, in that order. The delay between pulses A and B is τ and that between pulses B and C is T; the signal is emitted after pulse C during emission time t. This sequence of the excitation pulses is known as rephasing sequence because, in the presence of inhomogeneity in the sample, the signal is emitted as a photon echo. As shown in Fig. 2(b), the photon echo is emitted when $t = \tau$. Unless otherwise stated, the results presented in this paper are obtained from rephasing one-quantum 2DFT spectra, which are obtained by measuring the spectrally resolved signal as delay τ is scanned and taking a Fourier transform with respect to this delay.

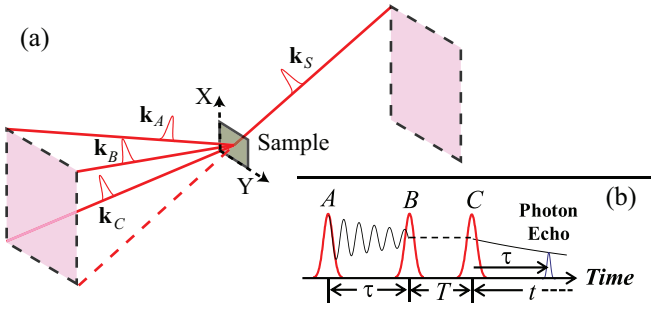

FIG. 2. (Color online) Schematic representation of excitation pulses A, B and C with wave vectors $\mathbf{k}_A$, $\mathbf{k}_B$ and $\mathbf{k}_C$, respectively, incident on the sample is shown in (a). The signal is emitted in the phase-matched direction $\mathbf{k}_S$. The X and Y directions are indicated on the sample. The rephasing pulse sequence is shown in (b). Pulse A is incident on the sample first followed by pulse B after a time interval τ. Pulse C impinges the sample next after delay T. In the presence of inhomogeneous broadening, the signal is emitted as a photon echo τ after pulse C.

Figure 3 shows the real part (a) and absolute value (b) of a typical rephasing 2DFT spectrum obtained for polarization scheme Y with the sample at a temperature of 10 K. The laser spectrum had a full width at half-maximum bandwidth of $\sim$ 16 meV and was tuned to be resonant with the HH exciton resonance. The dashed diagonal line in the spectrum marks equal absorption and emission energies. The vertical axis shows negative absorption energies since the phase evolution of the polarization during delay τ is opposite of that during t. In Fig. 3(a), the central dispersive peak (Ex) on the diagonal line is the HH exciton resonance. The negative absorptive peak (Bx) that is red-shifted relative to the exciton peak along the emission axis is due to the HH

bound biexciton state. The marked elongation of the HH exciton peak in the diagonal direction is because of large inhomogeneous broadening in the sample. The dispersive lineshape of the exciton peak suggests that the signal is dominated by many-body effects including EID and excitation-induced shift.[22]

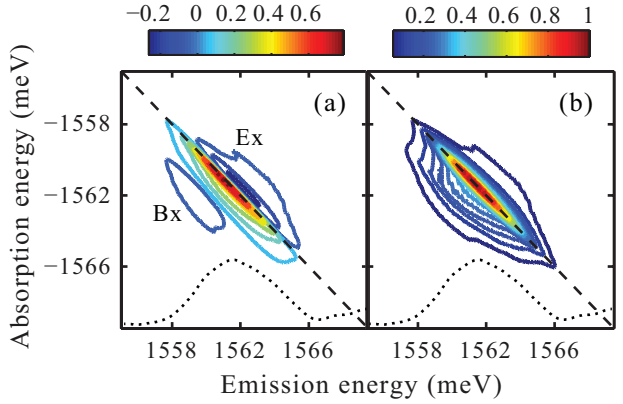

FIG. 3. (Color online) A typical real part (a) and absolute value (b) normalized 2DFT spectrum of the complex rephasing signal for polarization scheme Y and sample temperature of 10 K. The 2DFT spectra represent the third order nonlinear optical response of the system in two spectral dimensions. The 2DFT spectrum in (a) includes negative values since it shows the signal field radiated by the sample compared to the signal field amplitude shown in (b). The exciton (Ex) and biexciton (Bx) peaks are marked in (a). The dotted line at the bottom of the figures shows the linear absorption spectrum.

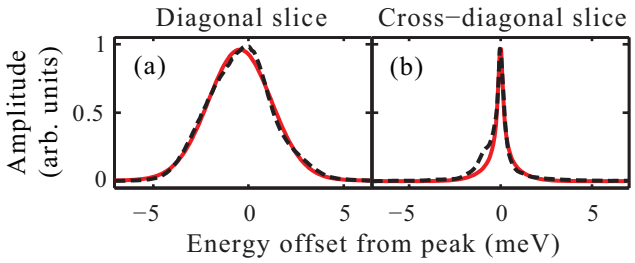

FIG. 4. (Color online) Slices (dashed line) and fits (solid line) along the diagonal (a) and cross-diagonal (b) directions of the normalized absolute value spectrum.

From an absolute value 2DFT spectrum, such as Fig. 3(b), the homogeneous and inhomogeneous linewidths are obtained by simultaneously fitting the diagonal and cross-diagonal slices to analytical lineshapes.[23] Figure 4 shows an example of the data (dashed line) and fit curves (solid line) for a 2DFT spectrum for polarization scheme Y. The sample was kept at a temperature of 10 K and the average photon density of $\sim 5.4 \times 10^{11}$ cm^{-2} per pulse was incident on it. There is a distinct difference between the cross-diagonal slice and the obtained fit on the negative energy wing of the main peak. This discrepancy is due to the weak biexciton peak which was not considered while performing the fits. For the slices shown in Fig. 4, we obtained values of 0.105 and 1.9 meV for the homogeneous and inhomogeneous linewidths, respectively. These, and the linewidths reported later on, are the half width at half-maximum (HWHM) values of the Lorentzian and Gaussian distribution functions, which correspond to homogeneous and inhomogeneous linewidths, respectively,[23] and have been obtained after deconvolution of the signal with the spectrometer response. The ratio of the linewidths suggest that inhomogeneity is the dominant broadening mechanism in (110)-oriented GaAs QWs. This result is expected from a rough growth front along the (110) direction for GaAs.[24]

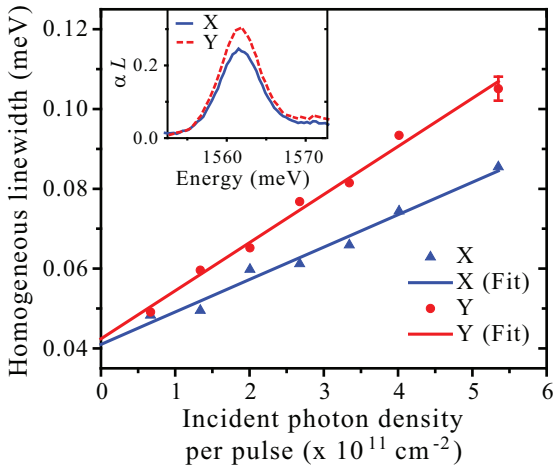

FIG. 5. (Color online) Incident photon density dependence of homogeneous linewidth for X (triangles) and Y (circles) polarization schemes. The linear fits to the data are shown by the solid lines. A representative error bar, obtained by repeating the same experiment multiple times, is shown. The inset shows the absorption spectrum for HH resonance for X (solid line) and Y (dashed line) polarizations. After subtracting out the bulk absorption in the substrate, the offset between the two absorption curves has been adjusted to have the same absorption for energies lower than the HH exciton resonance. For both the graph and the inset, the sample was kept at a temperature of 10 K.

On repeating the above measurement for polarization scheme X while keeping the other parameters the same, we measured a smaller homogeneous linewidth (0.086 meV) while the inhomogeneous linewidth was the same. We investigated the reason for unequal homogeneous linewidths for the two polarization schemes by varying the average photon density incident on the sample. Figure 5 shows the variation of the homogeneous linewidth with the average photon density per pulse incident on the sample kept at a temperature of 10 K, along with a representative error bar obtained by repeating the experiment multiple times. Over the range of photon density shown, the HH exciton state exhibits different homogeneous linewidths for X and Y polarization schemes. For both the polarization schemes, the homoge-

neous linewidth increases with increasing photon density due to EID,[25,26] while the inhomogeneous linewidth is constant at ~ 1.9 meV (data not shown).

For low photon density incident on the sample, the photon density dependence of the homogeneous linewidth can be approximated as[27]

$$\gamma(\phi) = \gamma_0 + \gamma_{EID} * \phi \quad (1)$$

where γ_0 is the zero-excitation density homogeneous linewidth, γ_{EID} is the rate of increase of homogeneous linewidth with average photon density per pulse ϕ incident on the sample. The solid lines in Fig. 5 are the fits to the data using Eqn. (1). The fit parameters listed in Table I show that while the value of γ_0 is the same (within the errors obtained by assuming constant error in homogeneous linewidth over the range of photon density), different values of γ_{EID} are obtained for the two polarization schemes.

Polarization scheme	γ_0 (μeV)	γ_{EID} (x 10^{-17} eVcm^2)
X	41 ± 2	8.1 ± 0.6
Y	42 ± 2	12.1 ± 0.5

TABLE I. Parameters of Eqn. (1) for the fits shown in Fig. 5.

In Eqn. (1), we use the average photon density per pulse incident on the sample rather than the exciton density in the QWs to quantify the effect of EID on the homogeneous linewidth. This is valid because, for relatively low photon density, the excitation density is directly proportional to the incident photon density. From the absorption spectra shown in the inset of Fig. 5, we estimate that the absorption of the HH exciton transition is ~ 1.3 times larger for Y polarization compared to X polarization. The difference in the exciton density for the same photon density incident on the sample results in different γ_{EID} values for the two polarization schemes. From the ratio of γ_{EID} for the two polarization schemes, we estimate an excitation density ratio of 1.5 ± 0.1 for polarization scheme Y to that for X. This ratio is in reasonable agreement with the estimate from the absorption curves and supports our analysis that anisotropic EID results in different homogeneous linewidth of the HH exciton transition polarized along X and Y axes.

For an electronic transition, both the absorption coefficient and the radiatively limited homogeneous linewidth are directly proportional to the square of the transition dipole moment.[28] Hence, if radiative decay was the only process contributing to γ_0, from unequal absorption coefficients for the HH exciton transitions polarized along X and Y axes, we would expect different γ_0 for the two polarizations. Equal values of γ_0 for both the polarizations suggest that it is not radiatively limited.

We can measure the population decay times from a rephasing zero-quantum 2DFT spectrum,[29,30] which is obtained by recording the spectrally resolved signal while scanning delay T and taking a Fourier transform with respect to the delay to get the mixing energy axis. Figure 6(a) shows such a 2DFT spectrum, for Y polarization scheme with the sample at a temperature of 10 K, where we plot the normalized signal intensity. When only a single resonance is excited, as is the case presently, the system is in a population state during T. Hence the linewidth in the mixing energy direction gives the population linewidth. We fit a slice from the zero-quantum 2DFT spectrum, indicated by the dashed line in Fig. 6(a), to a double Lorentzian. The linewidth of the narrower Lorentzian give the population lifetime. The slice (dashed line) and the best-fit curve (solid line) are shown in Fig. 6(b). We measure a population linewidth of ~ 10 μeV at a temperature of 10 K. We would like to point out that we did not measure different population linewidths for X and Y polarization schemes. However, due to ~ 2 μeV uncertainty in the population linewidths measured, we cannot confirm the presence of non-radiative population decay pathways. In the absence of pure dephasing mechanisms, the measured population linewidth would result in a homogeneous linewidth of $\sim$5 μeV for both X and Y polarization schemes. Since measured γ_0 is roughly 8 times this value, we can unambiguously conclude that pure dephasing processes contribute significantly to the measured γ_0. Exciton-phonon interaction is an important mechanism that contributes to the homogeneous linewidth in QWs. We investigate this

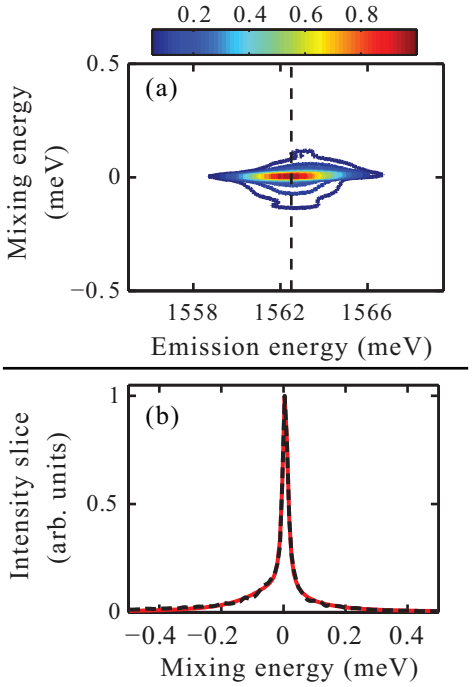

FIG. 6. (Color online) A rephasing zero-quantum 2DFT spectrum for Y polarization scheme is shown in (a). The spectrum plots signal intensity. The slice (dashed line) at the center of the inhomogeneous distribution of the spectrum in (a) is shown in (b). The solid line in (b) shows the best-fit double Lorentzian curve.

interaction through the temperature dependence of the homogeneous linewidth.

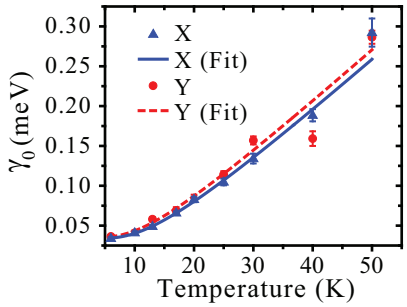

FIG. 7. (Color online) Sample temperature dependence of γ_0 for X (triangles) and Y (circles) polarization schemes. The fit, as per Eqn. (2), is represented by the solid (dashed) line for X (Y) polarization scheme. The error bars represent the statistical errors only and additional systematic error might also be present. Note that for a few temperatures the data points for X and Y polarization schemes overlap.

We repeated the power dependence study presented earlier for different sample temperatures varying from 6 to 50 K. We plot the values of γ_0 for X and Y polarization schemes for different temperatures in Fig. 7. For both the polarization schemes, nearly equal values of γ_0 are obtained over the temperature range studied as expected from the discussion of the anisotropic EID effect earlier. Additionally, we find that γ_0 increases with the sample temperature for both the polarization schemes. As the lattice temperature increases, exciton-phonon interactions increase resulting in a faster dephasing of excitons. Since, the phonon population follows the Bose - Einstein distribution, we can describe the thermal broadening as

$$\gamma_0(T_s) = \gamma_0(0) + \gamma^* \left[e^{\frac{E_{ph}}{k_B T_s}} - 1 \right]^{-1} \qquad (2)$$

where we have written γ_0 as a function of the sample temperature T_s, γ^* is the amplitude of the thermal dephasing term, E_{ph} is the energy of the dominant phonon mode responsible for the dephasing and k_B is the Boltzmann constant. In Eqn. (2) we have considered the contribution of only a single phonon mode to the pure dephasing of excitons. Equation (2) is similar to the one used by Lee *et al.*[31] for (001)-oriented GaAs QWs. The difference here is that we have not used the term that is linear in T_s, kept E_{ph} as an adjustable parameter and not considered impurity scattering effects. The best-fit curves are shown in Fig. 7 by a solid (dashed) line for polarization scheme X (Y). The values obtained for the fit parameters, which are equal for the two polarization schemes (within the errors), are listed in Table II.

We find the zero-excitation density homogeneous linewidth extrapolated to 0 K, $\gamma_0(0)$, is ~ 34 μeV (corresponding to a dephasing time of ~ 20 ps) and phonons with energy of ~ 3 meV are predominantly responsible

Polarization scheme	$\gamma_0(0)$ (μeV)	γ^* (meV)	E_{ph} (meV)
X	34 ± 2	0.24 ± 0.03	3.1 ± 0.3
Y	35 ± 4	0.22 ± 0.08	2.9 ± 0.7

TABLE II. Parameters of Eqn. (2) for the fits shown in Fig. 7.

for the faster dephasing of the HH exciton polarization at high temperatures. Usually E_{ph} corresponds to a transition to a real state which, in this case, could be delocalized exciton states centered ~ 3 meV above the line-center of the HH exciton inhomogeneous distribution. This activation would be an incoherent process that we can probe by varying the time delay between the second and third pulses.[32] We do not see any activation peak in these complimentary experiments (spectra not shown), which suggests that the thermal broadening is due to an elastic exciton-phonon scattering mediated virtual activation process. However, an activation peak too weak to be seen and/or activation to a dark state due to a change in the in-plane momentum of excitons cannot be ruled out. Equal values of γ^* and E_{ph} for both the polarization schemes suggest that the activation mechanism is isotropic for exciton transitions polarized along X and Y directions.

Compared with the population times reported earlier, the values of $\gamma_0(0)$ obtained for the two polarizations indicate that the HH exciton transition is dominated by pure dephasing processes even at low temperatures. We attribute this dephasing to acoustic phonon assisted tunneling of excitons between localization sites,[33] which exists due to disorder in the sample. This tunneling is important at low temperatures and does not show any activation-like behavior if it is accompanied with the emission of phonons.

We would like to point out that studies of temperature dependence of homogeneous linewidth of HH excitons in (001)-oriented GaAs QWs have shown[31,34–36] that at low temperatures (< 50 K) the linewidth increased linearly with temperature. This behavior would be replicated by Eqn. 2 for $E_{ph} \ll k_B T_s$. Thus, we conclude that for (001)-oriented GaAs QWs E_{ph} would be lesser than what we measure for the (110)-oriented QWs. We would also like to note that for (001)-oriented GaAs QWs with well widths ranging from 5 - 13 nm, low temperature dephasing times of 1-12 ps have been reported.[5,25,34,36,37] The homogeneous linewidth of excitons is sensitive to the inhomogeneity. As a consequence, the results in the publications cited above show quite large variation in dephasing times although all those results are for samples with relatively small inhomogeneous linewidth (HWHM < 0.5 meV). While the dephasing time we report here for (110)-oriented QWs is slightly longer than these values, it is smaller than the value of ~ 70 ps reported for (001)-oriented sample with significantly greater inhomogeneity.[3]

In conclusion, we have measured the linewidths of the

HH exciton resonance in (110)-oriented GaAs QWs. The measurements reveal that inhomogeneous broadening is the dominant broadening mechanism. In addition to reporting the dephasing time in a QW with reduced symmetry such as (110)-oriented GaAs QWs for the first time, we have also discussed important phenomena that affect the dephasing time. We show that anisotropic dipole moments along X and Y crystal axes, through EID, result in different homogeneous linewidths for exciton transitions polarized along the two axes. We find that the increase in homogeneous linewidth with temperature is isotropic along X and Y axes and shows an activation-like behavior, and that the homogeneous linewidth, even at low temperatures, is dominated by pure dephasing processes.

We acknowledge discussions with Mackillo Kira. The work at JILA was primarily supported by the Chemical Sciences, Geosciences, and Energy Biosciences Division, Office of Basic Energy Science, Office of Science, U.S. Department of Energy under Award# DE-FG02-02ER15346, as well NIST. G.N. acknowledges support by the Swiss National Science Foundation (SNSF). S.T.C. acknowledges funding from the Alexander von Humboldt Foundation.

* cundiff@jila.colorado.edu

[1] J. Shah, *Ultrafast Spectroscopy of Semiconductors and Semiconductor Nanostructures* (Springer, Berlin, 1999).
[2] Steven T. Cundiff, Opt. Express **16**, 4639 (2008).
[3] M. D. Webb, S. T. Cundiff, and D. G. Steel, Phys. Rev. Lett. **66**, 934 (1991).
[4] C. Weisbuch, R. Dingle, A. Gossard, and W. Wiegmann, Solid State Commun. **38**, 709 (1981).
[5] A. D. Bristow, T. Zhang, M. E. Siemens, S. T. Cundiff, and R. P. Mirin, J. Phys. Chem. B **115**, 5365 (2011).
[6] Y. Ohno, R. Terauchi, T. Adachi, F. Matsukura, and H. Ohno, Phys. Rev. Lett. **83**, 4196 (1999).
[7] G. M. Müller, M. Römer, D. Schuh, W. Wegscheider, J. Hübner, and M. Oestreich, Phys. Rev. Lett. **101**, 206601 (2008).
[8] H. Diehl, V. A. Shalygin, V. V. Bel'kov, Ch. Hoffmann, S. N. Danilov, T. Herrle, S. A. Tarasenko, D. Schuh, Ch. Gerl, W. Wegscheider, W. Prettl, and S. D. Ganichev, New J. Phys. **9**, 349 (2007).
[9] M. Bieler, IEEE J. Sel. Topics Quantum Electron. **14**, 458 (2008).
[10] A. Haché, Y. Kostoulas, R. Atanasov, J. L. P. Hughes, J. E. Sipe, and H. M. van Driel, Phys. Rev. Lett. **78**, 306 (1997).
[11] M. J. Stevens, A. L. Smirl, R. D. R. Bhat, A. Najmaie, J. E. Sipe, and H. M. van Driel, Phys. Rev. Lett. **90**, 136603 (2003).
[12] S. Priyadarshi, K. Pierz, and M. Bieler, Phys. Rev. Lett. **109**, 216601 (2012).
[13] M. Bieler, K. Pierz, U. Siegner, and P. Dawson, Phys. Rev. B **73**, 241312 (2006).
[14] S. Oertel, S. Kunz, D. Schuh, W. Wegscheider, J. Hübner, and M. Oestreich, Europhys. Lett. **96**, 67010 (2011).
[15] S. D. Ganichev and W. Prettl, J. Phys. Condens. Matter **15**, R935 (2003).
[16] H. T. Duc, J. Förstner, and T. Meier, Phys. Rev. B **82**, 115316 (2010).
[17] D. Gershoni, I. Brener, G. A. Baraff, S. N. G. Chu, L. N. Pfeiffer, and K. West, Phys. Rev. B **44**, 1930 (1991).
[18] S. Nojima, Phys. Rev. B **47**, 13535 (1993).
[19] S. Adachi, J. Appl. Phys. **58**, R1 (1985).
[20] S. T. Cundiff, J. Opt. Soc. Am. B **29**, A69 (2012).
[21] A. D. Bristow, D. Karaiskaj, X. Dai, T. Zhang, C. Carlsson, K. R. Hagen, R. Jimenez, and S. T. Cundiff, Rev. Sci. Instrum. **80**, 073108 (2009).
[22] X. Li, T. Zhang, C. N. Borca, and S. T. Cundiff, Phys. Rev. Lett. **96**, 057406 (2006).
[23] M. E. Siemens, G. Moody, H. Li, A. D. Bristow, and S. T. Cundiff, Opt. Express **18**, 17699 (2010).
[24] M. Yoshita, N. Kondo, H. Sakaki, M. Baba, and H. Akiyama, Phys. Rev. B **63**, 075305 (2001).
[25] A. Honold, L. Schultheis, J. Kuhl, and C. W. Tu, Phys. Rev. B **40**, 6442 (1989).
[26] H. Wang, K. Ferrio, D. G. Steel, Y. Z. Hu, R. Binder, and S. W. Koch, Phys. Rev. Lett. **71**, 1261 (1993).
[27] Y. Z. Hu, R. Binder, S. W. Koch, S. T. Cundiff, H. Wang, and D. G. Steel, Phys. Rev. B **49**, 14382 (1994).
[28] H. Haug and S. W. Koch, *Quantum Theory of the Optical and Electronic Properties of Semiconductors* (World Scientific, Singapore, 2009).
[29] Lijun Yang, Tianhao Zhang, Alan D. Bristow, Steven T. Cundiff, and Shaul Mukamel, J. Chem. Phys. **129**, 234711 (2008).
[30] G. Moody, R. Singh, H. Li, I. Akimov, M. Bayer, D. Reuter, A. Wieck, and S. Cundiff, Solid State Commun. **163**, 65 (2013).
[31] J. Lee, E. S. Koteles, and M. O. Vassell, Phys. Rev. B **33**, 5512 (1986).
[32] G. Moody, M. E. Siemens, A. D. Bristow, X. Dai, A. S. Bracker, D. Gammon, and S. T. Cundiff, Phys. Rev. B **83**, 245316 (2011).
[33] T. Takagahara, Phys. Rev. B **32**, 7013 (1985).
[34] L. Schultheis, A. Honold, J. Kuhl, K. Köhler, and C. W. Tu, Phys. Rev. B **34**, 9027 (1986).
[35] T. Ruf, J. Spitzer, V. F. Sapega, V. I. Belitsky, M. Cardona, and K. Ploog, Phys. Rev. B **50**, 1792 (1994).
[36] D. Gammon, S. Rudin, T. L. Reinecke, D. S. Katzer, and C. S. Kyono, Phys. Rev. B **51**, 16785 (1995).
[37] D. Birkedal, V. G. Lyssenko, J. M. Hvam, and K. El Sayed, Phys. Rev. B **54**, R14250 (1996).